FULL PAPER

Organic–Inorganic Perovskite Light-Emitting Electrochemical Cells with a Large Capacitance

Huimin Zhang, Hong Lin, Chunjun Liang,* Hong Liu, Jingjing Liang, Yong Zhao, Wenguan Zhang, Mengjie Sun, Weikang Xiao, Han Li, Stefano Polizzi, Dan Li, Fujun Zhang, Zhiqun He,* and Wallace C. H. Choy*

While perovskite light-emitting diodes typically made with high work function anodes and low work function cathodes have recently gained intense interests. Perovskite light-emitting devices with two high work function electrodes with interesting features are demonstrated here. Firstly, electroluminescence can be easily obtained from both forward and reverse biases. Secondly, the results of impedance spectroscopy indicate that the ionic conductivity in the iodide perovskite ($CH_3NH_3PbI_3$) is large with a value of $\approx 10^{-8}$ S cm^{-1}. Thirdly, the shift of the emission spectrum in the mixed halide perovskite ($CH_3NH_3PbI_{3-x}Br_x$) light-emitting devices indicates that I$^-$ ions are mobile in the perovskites. Fourthly, this work shows that the accumulated ions at the interfaces result in a large capacitance (≈ 100 μF cm^{-2}). The above results conclusively prove that the organic–inorganic halide perovskites are solid electrolytes with mixed ionic and electronic conductivity and the light-emitting device is a light-emitting electrochemical cell. The work also suggests that the organic–inorganic halide perovskites are potential energy-storage materials, which may be applicable in the field of solid-state supercapacitors and batteries.

H. Zhang, Dr. C. Liang, H. Liu, J. Liang,
Y. Zhao, M. Sun, W. Xiao, H. Li, Dr. D. Li,
Dr. F. Zhang, Prof. Z. He
Key Laboratory of Luminescence
and Optical Information
Ministry of Education
School of Science
Beijing Jiaotong University
Beijing 100044, P. R. China
E-mail: chjliang@bjtu.edu.cn; zhqhe@bjtu.edu.cn
H. Lin, Prof. W. C. H. Choy
Department of Electrical and Electronic Engineering
The University of Hong Kong
Pokfulam Road, Hong Kong
E-mail: chchoy@eee.hku.hk
Dr. W. Zhang
Lab of Printing and Packaging Material
and Technology-Beijing Area Major Laboratory
Beijing Institute of Graphic Communication
Beijing 102600, P. R. China
Prof. S. Polizzi
Department of Molecular Sciences and Nanosystems
Università Ca' Foscari Venezia
Via Torino 155/B, 30172 Mestre Venezia, Italy

1. Introduction

Low-temperature solution-processed organic–inorganic halide perovskites have drawn worldwide attention due to their remarkable performance in photovoltaic devices.[1–11] The high energy conversion efficiency is attributed to their long carrier lifetimes [12–15] and high photoluminescence efficiencies[15] of the hybrid perovskites. Recently, the materials also demonstrate interesting light-emitting properties. They exhibit amplified spontaneous light emission with low thresholds,[16] optically pump lasing,[17] and bright electroluminescence (EL) in perovskite light-emitting diodes (LEDs).[18,19] Organic–inorganic halide perovskites generate high color purity (full width at half maximum ≈ 30 nm) light. Also, the emission spectrum can be easily tuned from near-infrared to visible and ultraviolet by adjusting the bandgap with substitution of metal cations,[20] halide anions,[18,19] or organic ligands.[21] Therefore, the progress suggests a potential development of this unique class of materials into efficient, high color-purity and color-tunable light emitters for low-cost display, lighting, and optical communication applications. Perovskite LEDs require multiple layers, some of them processed by evaporation under high vacuum conditions.[19,22] Air-sensitive low work-function metals or electron injecting layers are needed for efficient charge carrier injection in the devices.[23] For example, Ca, Al, and Ag were commonly used as cathode in perovskite LEDs. However, Ca is highly chemically active, while Al and Ag also react with halide perovskites.[24]

Light-emitting electrochemical cells (LECs) are one of the simplest kinds of EL devices,[25] which are formed from just one active layer containing an emitter with ionic conductivity.[26] Light-emitting polymers mixed with solid electrolyte[27–29] and ionic transition-metal small-molecular complexes[30,31] are representative LEC materials. LECs operate at low bias voltages, which achieve high power efficiencies, and allow for high work function air-stable electrodes.[32] The movement of the ions in the active layer under an applied bias allows for efficient electron injection from high work function electrodes.

In this work, we demonstrated perovskite light-emitting devices with two high work function electrodes. Interestingly,

www.MaterialsViews.com

**ADVANCED
FUNCTIONAL
MATERIALS**
www.afm-journal.de

FULL PAPER

under both forward and reverse biases, $CH_3CH_3PbI_3$ (MAPbI$_3$) perovskite light-emitting devices show infrared EL emission, which can also be demonstrated in $CH_3CH_3PbBr_3$ (MAPbBr$_3$) light-emitting devices with green color EL. The impedance spectroscopy indicates that the ionic conductivity in MAPbI$_3$ is very large with a value of $\approx 10^{-8}$ S cm^{-1}, which unambiguously show that the perovskite MAPbI$_3$ is a solid electrolyte with mixed ionic and electronic conductivity. In addition, there is a shift in the emission spectrum in MAPbI$_{3-x}$Br$_x$ light-emitting device by changing bias, indicating that I$^-$ ions are mobile in the perovskites. The results confirm that the devices are LECs. Consequently, the work suggests that the organic–inorganic halide perovskites are potential electrochemical energy-storage materials, which may be applicable in the field of solid-state supercapacitors and batteries.

2. Results and Discussion

2.1. EL Properties of the Iodide Perovskite Light-Emitting Devices

Light-emitting devices have a structure of perovskite MAPbI$_3$ sandwiched between two high work function electrodes of
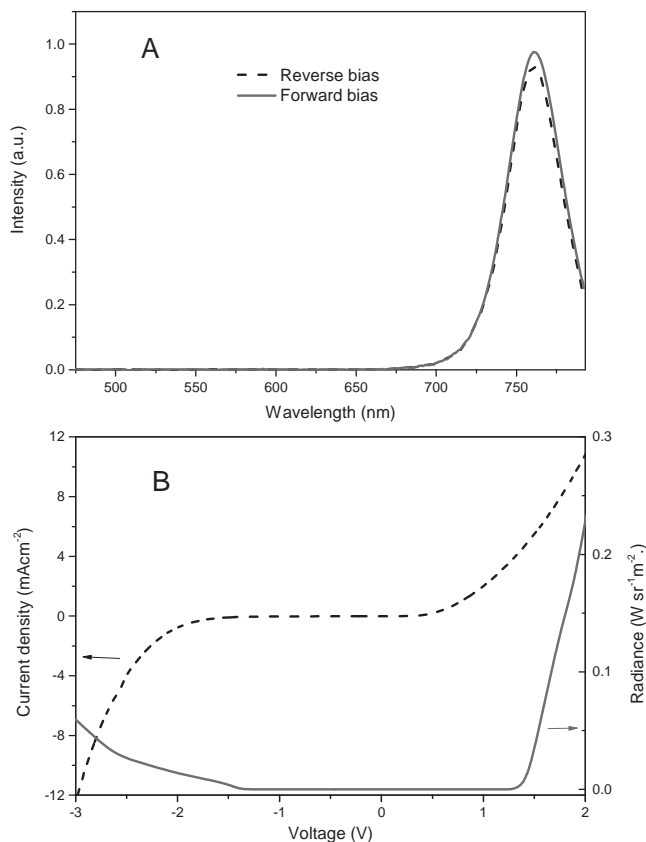
ITO/PEDOT:PSS and MoO$_3$/Au) (**Figure 1**A), with work function of 5.0 and 5.3 eV, respectively (Figure 1B). Light emission from the device at forward and reverse biases with the same EL spectra are observed as shown in **Figure 2**A. The emission of the iodide perovskite device is in the infrared region, with a peak at 761 nm and infrared radiance reaching 0.23 W sr^{-1} m^{-2} at the voltage of 2.0 V (MoO$_3$/Au is defined as the ground). The current density–voltage (*J–V*) curve (Figure 2B) shows symmetrical feature at forward and reverse biases, apparently violating the asymmetric conductance of conventional diodes. The threshold voltage for detection of light emission (Figure 2B) is ≈ 1.5 V for both forward-biased and reverse-biased scans. This turn-on voltage is close (in value) to the perovskite bandgap (1.5–1.6 eV). The abovementioned features are typical behavior of LECs,[27] which implies that the perovskite is a mixed electronic and ionic conductor.

2.2. Ionic Conduction Properties of the Iodide Perovskite

Impedance spectroscopy was used to distinguish the electronic and ionic components of conductivity in mixed conductors.[33] **Figure 3**A inset shows the equivalent circuit of the mixed conductor in the ITO/PEDOT:PSS/MAPbI$_3$/Au device. The
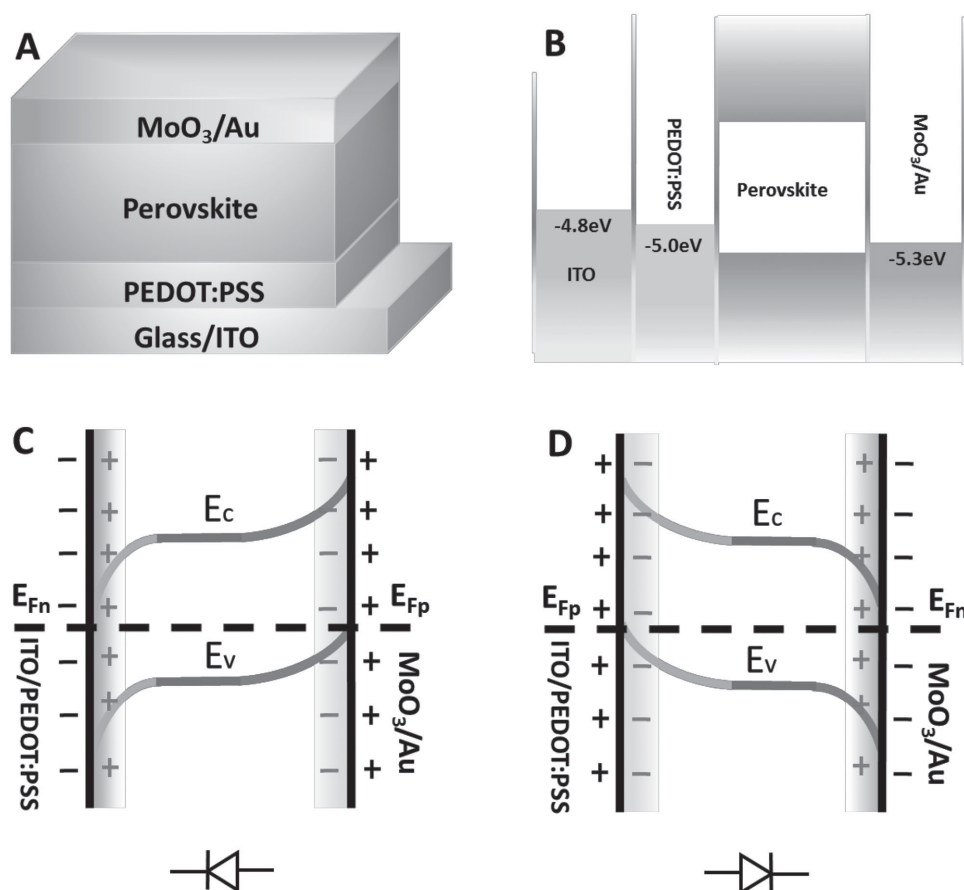
Figure 1. Device structure, energy level diagram, and the mechanism of the perovskite LECs. A) Device structure. B) Energy-level diagram of the materials. C) The device is a forward diode because of positive charge near the ITO/PEDOT:PSS electrode. D) The device is a reversed diode because of positive charge near the MoO$_3$/Au electrode. Interface charge and screen charge are represented in grey and black, respectively.

ADVANCED
FUNCTIONAL
MATERIALS
www.afm-journal.de

Materials
Views
www.MaterialsViews.com

FULL PAPER

Figure 2. EL properties of the iodide perovskite light-emitting devices. A) EL spectra of the device under forward and backward bias. B) Current–voltage and radiance–voltage characteristics of the device.

Table 1. A summary of the ionic conductivity, electronic conductivity, and the ionic transport number of MAPbI₃ at different temperatures.
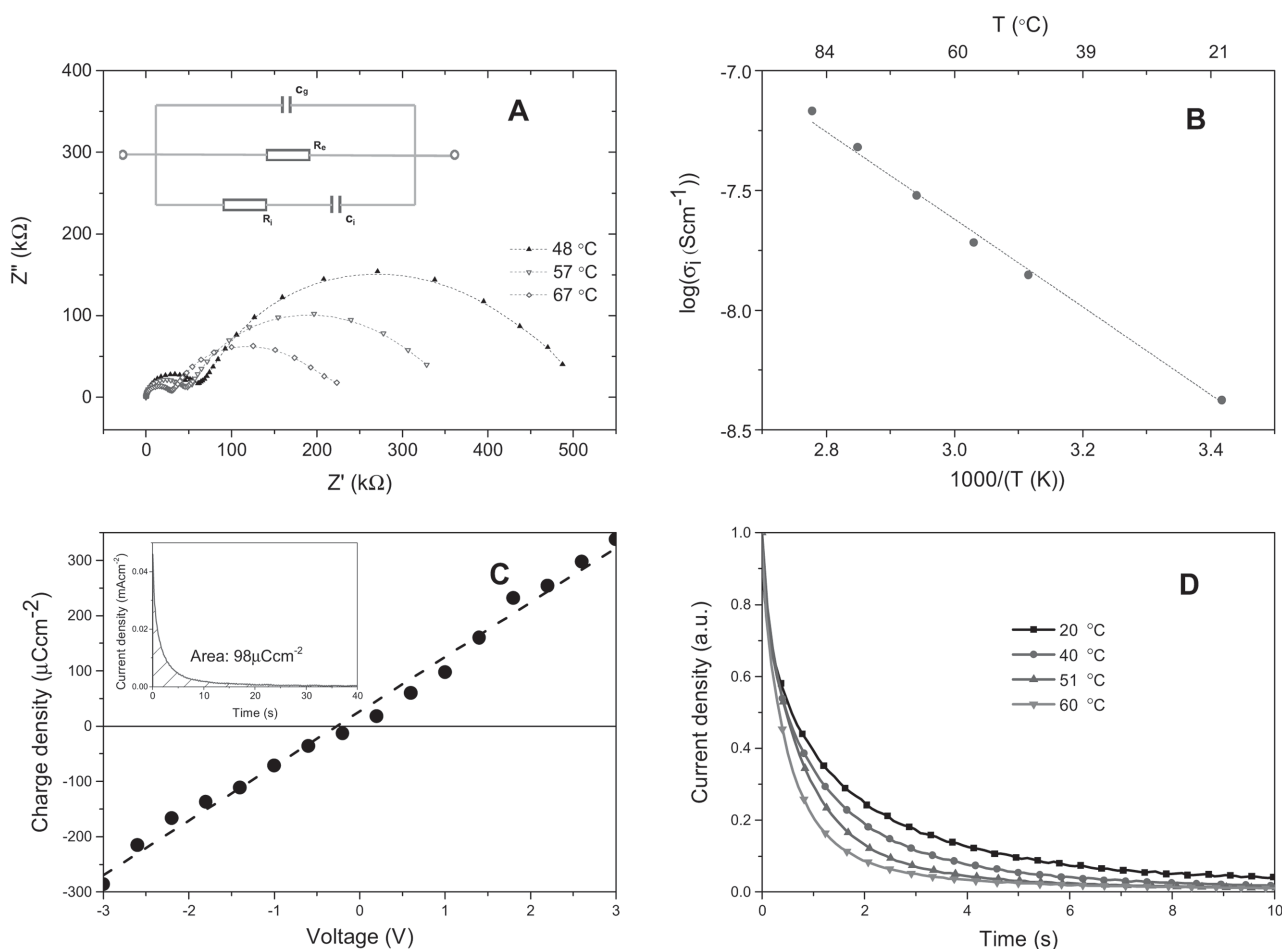
Temperature T [°C]	Ionic conductivity σ_i ($\times 10^{-9}$ [S cm^{-1}])	Electronic conductivity σ_e ($\times 10^{-9}$ [S cm^{-1}])	Ionic transport number t_i
20	4.2	1.3	0.76
48	14	2.2	0.87
57	19	3.1	0.86
67	30	4.7	0.87
78	47	8.0	0.86
87	68	12	0.84

that the activation energy of mobile ions in MAPbI₃ is 0.30 eV, which is very close to the activation energy for the migration of the vacancy of halide ions (0.29 eV) in inorganic halide perovskite (CsPbCl₃).[35]

A certain bias (e.g., 1.0 V) was applied on the device for a period of time (≈15 s) under dark condition to accumulate the ions; in other words, to charge C_i. The device was then rapidly switched to zero bias to measure the discharge current (Figure 3C, inset). The accumulated charge density at the bias (1.0 V) is the time integral of the discharge current. Figure 3C shows the measured charge densities of the accumulated ions at the interfaces under various biases. The slope of the curve indicates C_i value of ≈100 µF cm⁻². This large areal capacitance exceeds that of conventional electrostatic capacitors[36] with a typical value of 0.1 µF cm⁻², which is understandable because C_i is the capacitance between the solid perovskite electrolyte and the electrodes. The results suggest a potential application as solid-state supercapacitors by using the organic–inorganic perovskites. In the state-of-the-art supercapacitor design,[37] the conducting materials that have extremely large surface area, such as carbon nanotube or graphene, are used as electrodes. The surface area S of the electrode material can reach ≈1000 m² g⁻¹.[38] This could lead to a specific capacitance of C_s = SC_i = 1000 F g⁻¹ by using the perovskite material as the solid electrolyte, which is an attractive value for solid-state supercapacitors. However, great effort is still needed to improve the ionic conductivity and the ionic transport number (to unity) before making feasible devices.

The accumulation and relaxation of the interface charge are respectively the charge and discharge processes of C_i. Therefore, the RC constant of the ionic-conducting path, R_iC_i, governs the dynamics of the interface charge. For example, at the temperature of 20 °C, σ_i = 4.2 × 10⁻⁹ S cm⁻¹, using a thickness of L = 400 nm, and a capacitance of C_i = 100 µF cm⁻², then the time constant will be $R_iC_i = C_iL/\sigma_i \approx$ 1.0 s, which explains the time scale (in the range of seconds) of the discharge process as indicated in Figure 3D. The figure also shows the discharge process at different temperatures. Apparently, higher temperature leads to faster discharge because of the increased ionic conductivity and thus smaller RC constant at higher temperature.

The above results unambiguously indicate that the perovskite MAPbI₃ is a solid electrolyte with mixed ionic and electronic conductivity and thus confirm that the iodide perovskite light-emitting device is LEC. The accumulated ions at the interfaces change the band bending of the semiconductor and

electrodes in this device are ionically blocking but electronically conducting. Therefore, three parallel paths in the circuit are present. R_e is the resistance of the electronic-conducting path, R_i is the resistance of the ionic-conducting path, and C_i is the capacitance from the blocking of ions at the electrode interfaces. C_i represents the combined capacitive properties of the two electrolyte/electrode interfaces. C_g is the geometrical capacitance.

Figure 3A shows the Nyquist plot of the impedance spectra of the device at various temperatures. The curves with two adjacent semicircles on the complex impedance plane are typical behavior of solid electrolytes with mixed ionic and electronic conductivity. R_e and R_i determine the size of the semicircles (Figure S1, Supporting Information). The decrease in circle size with increasing temperature indicates that the conductivities increase at higher temperature. The ionic conductivity, electronic conductivity, and ionic transport number, which is the ratio of ionic conductivity and total conductivity, are calculated according to the size of the semicircles (see the Supporting Information) and summarized in **Table 1**. The ionic conductivity in MAPbI₃ is in the order of 10⁻⁸ S cm⁻¹, which is comparable with that in polymer electrolytes.[34] The ionic transport number is ≈0.8, which indicates that the ionic component dominates the conductivity.

Figure 3B shows the Arrhenius plot of the ionic conductivity at different temperatures. The slope of the plot indicates

www.MaterialsViews.com

ADVANCED
FUNCTIONAL
MATERIALS
www.afm-journal.de

FULL PAPER

Figure 3. Ionic behaviors of the perovskite MAPbI3. A) Nyquist plot of the impedance spectra at different temperatures. The inset shows the equivalent circuit. B) Ionic conductivity as a function of temperature. C) Measured interface charge density at various biases. D) The dynamics of the discharge process at different temperatures.

lead to polarity-switchable diodes (Figure 1C,D) which explains the EL at forward and reverse biases. The responsive time of the LECs is in the range of seconds (Figure S5, Supporting Information).

Since the results show that organic–inorganic perovskites are solid electrolyte, a device with the structure of electrode (1)/perovskite/electrode (2) can function as an electrochemical cell, suggesting that it is possible to measure the open-circuit electromotive force (EMF) in the cells with different electrode potentials.[35] We observed significant EMF in the device of ITO/PEDOT:PSS/MAPbI$_3$/PCBM/Au. Right after the device fabrication, we measured the open-circuit EMF (voltage) of the device under dark condition. **Figure 4**A shows the measured EMF of the device at various temperatures. Figure 4B shows the observed EMF and the short-circuit current of the device at room temperature under dark condition. The device shows significant EMF of ≈0.5 V and the apparent dark short-circuit current of ≈0.04 µA cm^{-2}. It is interesting to note that besides the report of the perovskite device of ITO/PEDOT:PSS/ MAPbI3/PCBM/Au as an efficient solar cell and light-emitting diode, the result of EMF indicates that perovskite device can work as a battery.

2.3. Shift of Emission Spectrum and Ion Migration of Mixed Bromide–Iodide Perovskite LECs

LECs are fabricated to obtain the light emission in visible range by using MAPbBr$_3$ and MAPbI$_{3-x}$Br$_x$ as emitters. The emission from the LECs of ITO/PEDOT:PSS (30 nm)/MAPbBr$_3$ (400 nm)/MoO$_3$ (8 nm)/Au is green, with the emission peak at 532 nm (**Figure 5**A). The turn-on voltage of the device is 2.4 V, which corresponds to the bandgap (≈2.4 eV) of the bromide perovskite.

The EL spectra of the mixed iodide–bromide perovskite LECs of ITO/PEDOT:PSS/MAPbI$_{3-x}$Br$_3$ (400 nm)/MoO$_3$/Au are tunable with the applied voltage (Figure 5B). At 2.0 V, the emission peaks at 743 nm, which is consistent with the photoluminescent (PL) spectrum of the mixed perovskite film with I-to-Br molar ratio of 4:9 (Figure 5C). When the voltage is increased, the peak continuously broadens at its shorter wavelength up to 5.0 V, and eventually shifts to 710 nm at 7.0 V. Another emission peak at 532 nm (the same peak as MAPbBr$_3$) appears at 5.0 V and becomes evidently pronounced at higher voltage.

The absorption and PL spectra of the materials with various I-to-Br ratios are investigated to understand the spectra shift.

FULL PAPER
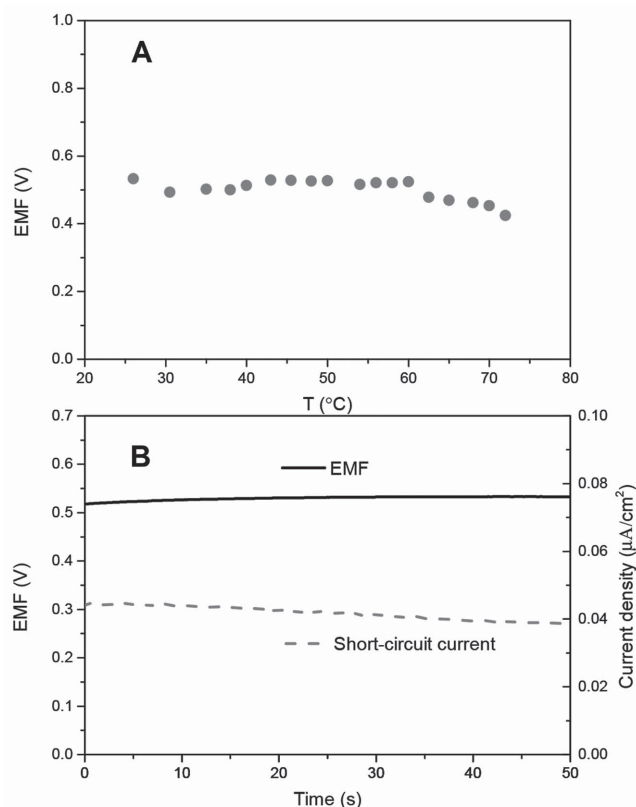
Figure 4. Electromotive force and the short-circuit current of the device ITO/PEDOT:PSS/MAPbI$_3$/PCBM/Au under dark condition. A) Electromotive force at various temperatures. B) Electromotive force and short-circuit current at room temperature.

The bandgap (Figure S3C, Supporting Information) and the PL emission (Figure 5C) of the mixed perovskite are continuously tunable with the I-to-Br ratio. At the I-to-Br ratio of 4:9, the PL emission peaks at 743 nm, which is consistent with the EL emission of the LECs at 2.0 V (Figure 5B). However, when the I-to-Br ratio decreases from 4:9 to 1:9, the PL emission peak shifts from 743 to 710 nm. This trend is similar to the peak shift in the LECs with increasing bias, implying that the spectra shift of the mixed perovskite LECs is due to the compositional change of the material in emission zone. At higher voltage, the I-to-Br ratio becomes lower and even iodine-free in some parts. Thus, this phenomenon leads to the blue shift of the emission in the infrared range and the appearance of the 532 nm emission band, which suggests that the halide ions, especially I$^-$ ions, are mobile in the perovskites. Under low bias, limited number of ions migrates to the interfaces. However, at higher bias, more ions, especially I$^-$ ions, drift toward the interface region, leading to the composition (I-to-Br ratio) change in the middle emission zone and thus the EL spectra shift (Figure S4, Supporting Information).

This hypothesis is further confirmed by examining the EL spectra of the mixed perovskite in a different ITO/PEDOT:PSS/MAPbI$_{3-x}$Br$_x$ (MAI-40 mg mL^{-1})/PCBM/Au device (Figure 5D). In this device, a thick PCBM layer (90 nm) was inserted between the perovskite and the Au electrode. As a consequence, significantly lower interface charge was observed,[39]

compared with the former mixed perovskite LECs (Figure S2, Supporting Information). This result indicates that at the same voltage, fewer ions migrate to the interface of the device. In contrast to the radical change in EL spectra in the former LECs, the peak shift in this device is very limited (from 745 to 742 nm), and no appearance of the 532 nm peak was observed when the bias was increased from 2.0 to 6.0 V. Therefore, the halide ions, especially I$^-$ ions, are mobile in the perovskite, and the spectra shift reflects the change in composition (I-to-Br ratio) of the mixed perovskites under different biases. This result agrees with the theoretical one of MAPbI$_3$ determined by density functional theory recently[40] and previous experimental finding that ionic conduction is caused by the migration of halide-ion vacancies (Figure S6, Supporting Information) in inorganic halide perovskites[35] and in organic–inorganic halide perovskite CH$_3$NH$_3$GeCl$_3$.[41]

3. Conclusions

In this work, we demonstrate EL of perovskite light-emitting devices with two high work function electrodes under both forward and reverse biases. The shift of emission spectrum of MAPbI$_{3-x}$Br$_x$ perovskite light-emitting device indicates that I$^-$ ions move in the perovskite during operation. Meanwhile, the results of impedance spectroscopy indicate that MAPbI$_3$ is a solid electrolyte with mixed ionic and electronic conductivity. The ionic conductivity in MAPbI$_3$ is ≈10^{-8} S cm^{-1}, and the ionic transport number is ≈0.8. The activation energy for the migration of ions in the organic–inorganic halide perovskite is 0.30 eV. We also observed significant electromotive force in perovskite devices. The results confirm that the perovskite light-emitting devices with two high work function electrodes are LECs. The extremely simple device structure and the use of high work function electrode further strengthen the potential of developing the organic–inorganic perovskite into efficient, high color-purity and color-tunable light emitters for low-cost display, lighting, and optical communication applications.

In addition, the above results suggest new applications for organic–inorganic halide perovskites. Besides the demonstrated light-emitting electrochemical device, the significant ionic conductivity also suggests the potential application of electrochemical energy-storage devices,[42] such as solid-state supercapacitors and batteries. The observed large capacitance (≈100 µF cm^{-2}) and the significant EMF of perovskite devices support this suggestion. Therefore, it is possible to build an integrated device including photovoltaic energy harvesting, energy storage, and light-emitting subparts all from organic–inorganic perovskites.

4. Experimental Section

PbI$_2$ and PbBr$_2$ were dissolved in DMF (1 M) and CH$_3$NH$_3$I (MAI) was dissolved in 2-propanol. To ensure MAI, PbBr$_2$, and PbI$_2$ were fully dissolved, both solutions were heated at 70 °C for 30 min before use. The device architecture were ITO/PEDOT:PSS (30 nm)/MAPbI$_3$ (400 nm)/Au, ITO/PEDOT:PSS (30 nm)/MAPbI$_3$ (400 nm)/MoO$_3$ (8 nm)/Au, and ITO/PEDOT:PSS (30nm)/MAPbI$_{3-x}$Br$_x$ (400 nm)/MoO$_3$ (8 nm)/Au. The active area is 0.038 cm^2. PEDOT:PSS (Baytron-P4083)
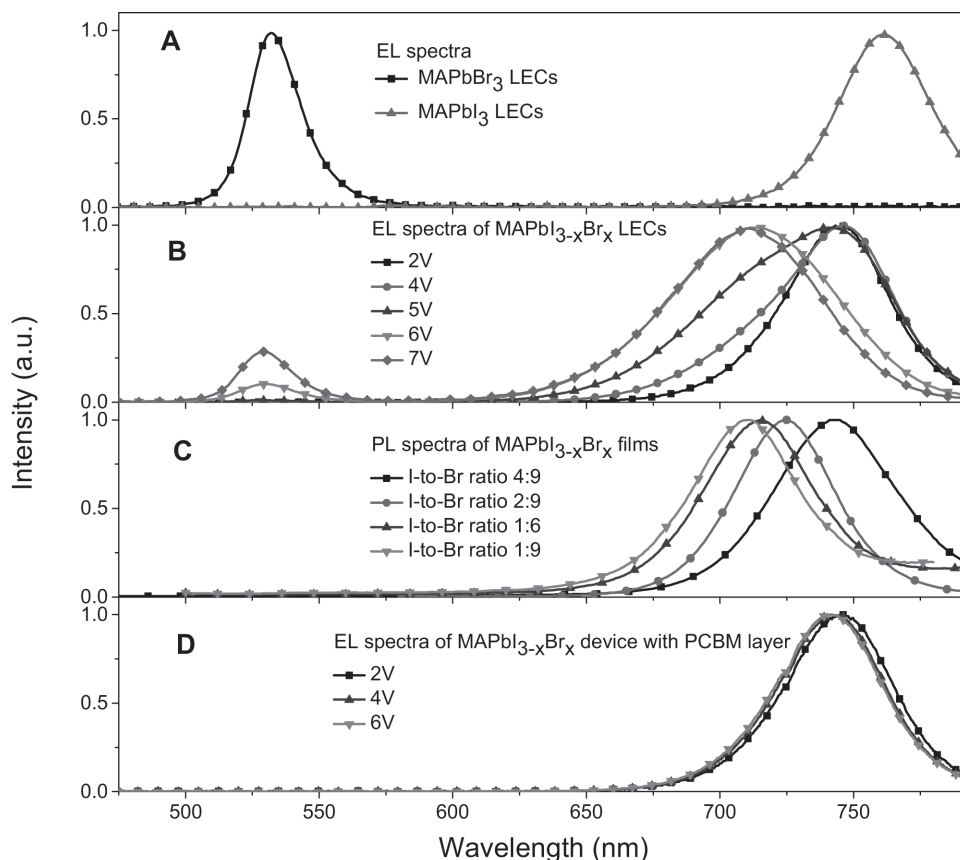
Figure 5. EL and PL spectra of bromide perovskite and mixed iodide–bromide perovskite. A) EL spectra of MAPbI$_3$ and MAPbBr$_3$ in the LECs of ITO/PEDOT:PSS/Perovskite/MoO$_3$/Au. B) EL spectra of the mixed perovskite MAPbI$_{3-x}$Br$_x$ in the LECs of ITO/PEDOT:PSS/Perovskite/MoO$_3$/Au at different biases. C) PL spectra of the mixed perovskite MAPbI$_{3-x}$Br$_x$ with different I-to-Br ratios. D) EL spectra of the mixed perovskite MAPbI$_{3-x}$Br$_x$ in the device ITO/PEDOT:PSS/Perovskite/PCBM/Au at different biases.

was spin-cast onto the clean surface of the ITO substrates at 4000 rpm for 40 s and then thermally annealed on a hot plate at 120 °C for 30 min in air. In a nitrogen-filled glove box, the solution of PbI$_2$ was spin-coated onto the PEDOT:PSS layer at 4000 rpm for 15 s and then annealed at 70 °C for 15 min. After drying, the MAI solution in 2-propanol (20 mg mL^{-1}) was spin-coated onto the PbI$_2$ layer at 3000 rpm for 5 s and then annealed at 70 °C for 30 min to form the perovskite MAPbI$_3$. The solution of PbBr$_2$ was spin-coated onto the PEDOT:PSS layer at 4000 rpm for 15 s and then annealed at 70 °C for 15 min. After drying, the MAI solution with different concentration in 2-propanol (40 mg mL^{-1}) was spin-coated onto the PbBr2 layer at 3000 rpm for 5 s and then annealed at 70 °C for 30 min to form the perovskite MAPbI$_{3-x}$Br$_x$. PC$_{61}$BM (in chlorobenzene) was then spin-coated onto the perovskite layer at 3000 rpm for 40 s. Finally, the samples were moved into a vacuum chamber for MoO$_3$ and gold deposition. The thickness of the MoO$_3$ and gold are 8 and 80 nm, respectively. The thickness of the perovskite is ≈400 nm, as measured with an Ambios XP-2 profilometer. The *J–V* characteristics were recorded by a Keithley (and Agilent) source meter under dark condition. The PL spectra of the perovskite films were recorded by a Fluorolog-3 fluorescence spectrometer. The EL spectra were recorded by an Acton Insectrum CCD spectrometer. The radiance of the infrared emission was measured with a Newport Optical Power Meter. Impedance spectroscopy was conducted on a Zahner Zennium electrochemical workstation. The impedance spectra were measured under a small AC signal with an amplitude of 20 mV at the bias of 0 V under dark condition. The detailed method to calculate the ionic conductivity, the electronic conductivity, and the ionic transport number is available in the Supporting Information.

Supporting Information

Supporting Information is available from the Wiley Online Library or from the author.

Acknowledgements

[1] A. Kojima, K. Teshima, Y. Shirai, T. Miyasaka, *J. Am. Chem. Soc.* **2009**, *131*, 6050.
[2] D. Liu, T. L. Kelly, *Nat. Photon.* **2014**, *8*, 133.

FULL PAPER

[3] H. Zhou, Q. Chen, G. Li, S. Luo, T. B. Song, H. S. Duan, Z. Hong, J. You, Y. Liu, Y. Yang, *Science* **2014**, *345*, 542.

[4] S. Sun, T. Salim, N. Mathews, M. Duchamp, C. Boothroyd, G. Xing, T. C. Sum, Y. M. Lam, *Energy Environ. Sci.* **2014**, *7*, 399.

[5] Z. Xiao, C. Bi, Y. Shao, Q. Dong, Q. Wang, Y. Yuan, C. Wang, Y. Gao, J. Huang, *Energy Environ. Sci.* **2014**, *7*, 2619.

[6] S. Ryu, J. H. Noh, N. J. Jeon, Y. C. Kim, S. Yang, J. W. Seo, S. I. Seok, *Energy Environ. Sci.* **2014**, *7*, 2614.

[7] B. Conings, L. Baeten, C. De Dobbelaere, J. D'Haen, J. Manca, H.-G. Boyen, *Adv. Mater.* **2014**, *26*, 2041.

[8] J. You, Z. Hong, Y. Yang, Q. Chen, M. Cai, T.-B. Song, C.-C. Chen, S. Lu, Y. Liu, H. Zhou, Y. Yang, *ACS Nano* **2014**, *8*, 1674.

[9] J.-Y. Jeng, K.-C. Chen, T.-Y. Chiang, P.-Y. Lin, T.-D. Tsai, Y.-C. Chang, T.-F. Guo, P. Chen, T.-C. Wen, Y.-J. Hsu, *Adv. Mater.* **2014**, *26*, 4107.

[10] F. X. Xie, D. Zhang, H. Su, X. Ren, K. S. Wong, M. Grätzel, W. C. H. Choy, *ACS Nano* **2015**, *9*, 639.

[11] W. E. I. Sha, X. Ren, L. Chen, W. C. H. Choy, *Appl. Phys. Lett.* **2015**, *106*, 221104.

[12] S. D. Stranks, G. E. Eperon, G. Grancini, C. Menelaou, M. J. Alcocer, T. Leijtens, L. M. Herz, A. Petrozza, H. J. Snaith, *Science* **2013**, *342*, 341.

[13] G. Xing, N. Mathews, S. Sun, S. S. Lim, Y. M. Lam, M. Gratzel, S. Mhaisalkar, T. C. Sum, *Science* **2013**, *342*, 344.

[14] D. Li, C. Liang, H. Zhang, C. Zhang, F. You, Z. He, *J. Appl. Phys.* **2015**, *117*, 074901.

[15] D. W. de Quilettes, S. M. Vorpahl, S. D. Stranks, H. Nagaoka, G. E. Eperon, M. E. Ziffer, H. J. Snaith, D. S. Ginger, *Science* **2015**, *348*, 683.

[16] G. Xing, N. Mathews, S. S. Lim, N. Yantara, X. Liu, D. Sabba, M. Gratzel, S. Mhaisalkar, T. C. Sum, *Nat. Mater.* **2014**, *13*, 476.

[17] F. Deschler, M. Price, S. Pathak, L. E. Klintberg, D.-D. Jarausch, R. Higler, S. Hüttner, T. Leijtens, S. D. Stranks, H. J. Snaith, M. Atatüre, R. T. Phillips, R. H. Friend, *J. Phys. Chem. Lett.* **2014**, *5*, 1421.

[18] Z.-K. Tan, R. S. Moghaddam, M. L. Lai, P. Docampo, R. Higler, F. Deschler, M. Price, A. Sadhanala, L. M. Pazos, D. Credgington, F. Hanusch, T. Bein, H. J. Snaith, R. H. Friend, *Nat. Nanotechnol.* **2014**, *9*, 687.

[19] Y. H. Kim, H. Cho, J. H. Heo, T. S. Kim, N. Myoung, C. L. Lee, S. H. Im, T. W. Lee, *Adv. Mater.* **2015**, *27*, 1248.

[20] F. Hao, C. C. Stoumpos, D. H. Cao, R. P. H. Chang, M. G. Kanatzidis, *Nat. Photon.* **2014**, *8*, 489.

[21] N. J. Jeon, J. H. Noh, W. S. Yang, Y. C. Kim, S. Ryu, J. Seo, S. I. Seok, *Nature* **2015**, *517*, 476.

[22] X. Qin, H. Dong, W. Hu, *Sci. China Mater.* **2015**, *58*, 186.

[23] G. Li, Z. K. Tan, D. Di, M. L. Lai, L. Jiang, J. H. Lim, R. H. Friend, N. C. Greenham, *Nano Lett.* **2015**, *15*, 2640.

[24] Z. Xiao, Y. Yuan, Y. Shao, Q. Wang, Q. Dong, C. Bi, P. Sharma, A. Gruverman, J. Huang, *Nat. Mater.* **2015**, *14*, 193.

[25] A. Sandstrom, H. F. Dam, F. C. Krebs, L. Edman, *Nat. Commun.* **2012**, *3*, 1002.

[26] Z. Yu, L. Li, H. Gao, Q. Pei, *Sci. China: Chem.* **2013**, *56*, 1075.

[27] Q. Pei, G. Yu, C. Zhang, Y. Yang, A. J. Heeger, *Science* **1995**, *269*, 1086.

[28] J. Gao, J. Dane, *Appl. Phys. Lett.* **2003**, *83*, 3027.

[29] X. Li, F. AlTal, G. Liu, J. Gao, *Appl. Phys. Lett.* **2013**, *103*, 243304.

[30] J. D. Slinker, J. Rivnay, J. S. Moskowitz, J. B. Parker, S. Bernhard, H. D. Abruna, G. G. Malliaras, *J. Mater. Chem.* **2007**, *17*, 2976.

[31] Y. Shen, D. D. Kuddes, C. A. Naquin, T. W. Hesterberg, C. Kusmierz, B. J. Holliday, J. D. Slinker, *Appl. Phys. Lett.* **2013**, *102*, 203305.

[32] S. B. Meier, D. Tordera, A. Pertegás, C. Roldán-Carmona, E. Ortí, H. J. Bolink, *Mater. Today* **2014**, *17*, 217.

[33] R. A. Huggins, *Ionics* **2002**, *8*, 300.

[34] Z. Gadjourova, Y. G. Andreev, D. P. Tunstall, P. G. Bruce, *Nature* **2001**, *412*, 520.

[35] J. Mizusaki, K. Arai, K. Fueki, *Solid State Ionics* **1983**, *11*, 203.

[36] P. Sharma, T. S. Bhatti, *Energy Convers. Manage.* **2010**, *51*, 2901.

[37] X. Lu, M. Yu, G. Wang, Y. Tong, Y. Li, *Energy Environ. Sci.* **2014**, *7*, 2160.

[38] J. R. Miller, P. Simon, *Interface* **2008**, *17*, 2.

[39] H. Zhang, C. Liang, Y. Zhao, M. Sun, H. Liu, J. Liang, D. Li, F. Zhang, Z. He, *Phys. Chem. Chem. Phys.* **2015**, *17*, 9613.

[40] C. Eames, J. M. Frost, P. R. Barnes, B. C. O'Regan, A. Walsh, M. S. Islam, *Nat. Commun.* **2015**, *6*, 7497.

[41] K. Yamada, K. Isobe, E. Tsuyama, T. Okuda, Y. Furukawa, *Solid State Ionics* **1995**, *79*, 152.

[42] K. Funke, *Sci. Technol. Adv. Mater.* **2013**, *14*, 043502.